Desalination and Water Treatment
www.deswater.com

doi: 10.5004/dwt.2020.26247

204 (2020) 136–143
November

Physicochemical characterization of La-doped g-C_3N_4 for degradation of phenol and organic dye

A. Bouzidi[a], Mai S.A. Hussien[b,c], Hisham S.M. Abd-Rabboh[d,e], Ayman A.H. Abdelrhim[d,f], I.S. Yahia[c,g,h], Nasser S. Awwad[d,*]

[a]*Research Unit, Physics of Insulating and Semi-insulating Materials, Faculty of Sciences, University of Sfax, B.P. 1171, 3000 Sfax, Tunisia, email: bouzidi.abdelfatteh@yahoo.fr (A. Bouzidi)*
[b]*Department of Chemistry, Faculty of Education, Ain Shams University, Roxy, 11757 Cairo, Egypt, email: maisalehamar@gmail.com (M.S.A. Hussien)*
[c]*Nanoscience Laboratory for Environmental and Bio-medical Applications (NLEBA), Semiconductor Laboratory and Department of Physics, Faculty of Education, Ain Shams University, Roxy, 11757 Cairo, Egypt, email: dr_isyahia@yahoo.com (I.S. Yahia)*
[d]*Department of Chemistry, Faculty of Science, King Khalid University, P.O. Box: 9004, Abha, Saudi Arabia, Tel. +966 549323204; emails: aawwad@kku.edu.sa (N.S. Awwad), hasalah@hotmail.com (H.S.M. Abd-Rabboh), aymanabdelrhim@gmail.com (Ayman A.H. Abdelrhim)*
[e]*Department of Chemistry, Faculty of Science, Ain Shams University, Abbassia, 11566 Cairo, Egypt*
[f]*Department of Industrial Design–Faculty of Applied Arts–Damietta University, Damietta, Egypt*
[g]*Advanced Functional Materials and Optoelectronic Laboratory, Department of Physics, Faculty of Science, King Khalid University, P.O. Box: 9004, Abha, Saudi Arabia*
[h]*Research Center for Advanced Materials Science (RCAMS), King Khalid University, Abha 61413, P.O. Box: 9004, Saudi Arabia*

Received 3 September 2019; Accepted 9 June 2020

ABSTRACT

A series of La-doped (0.001–1 g) graphitic carbon nitride (g-C_3N_4) samples was prepared through the air atmospheric pyrolysis of melamine. Different analytical techniques were employed to characterize the structural, morphological, optical, and photocatalytic properties of both pure and doped g-C_3N_4 samples. The phase structures of pure and La-doped g-C_3N_4 samples were revealed by X-ray diffraction. The scanning electron microscopy analysis expressed that the well-defined particle shape became ambiguous, and the particle size gradually decreased with the increasing doping amount of La nitrate ions. Due to La doping on g-C_3N_4, the optical properties of the samples were improved. In comparison to pure g-C_3N_4, La-doped g-C_3N_4 manifested higher photocatalytic degradation efficiency toward methylene blue (MB) and phenol under visible light irradiation.

Keywords: Graphitic carbon nitride; Photocatalytic efficiency; Pyrolysis; La nitrate ions; Phenol; Methylene blue

1. Introduction

Population growth and continuously rising living standards over the last decades have caused a dramatic increase in energy consumption all over the world [1]. Consequently, a rapid decrease in fossil fuel sources and an increase in pollution and the use of renewable energy sources have also noticed. Researchers have adopted different technologies to efficiently use clean and limitless solar energy. Photocatalysts harvest solar energy to improve the efficiency of solar cells [2]. As a light-emitting diode, a fuel cell electrode, and a photocatalyst, non-oxide lightweight carbon nitride (C_3N_4) is a promising material for different applications, and numerous preparation and characterization

* Corresponding author.

methods of C_3N_4 have been proposed in recent years [3–5]. The quest for suitable new energy resources and pollution-degradation strategies has become an important research topic to solve the current energy crisis and environmental problems. As a pollution-free and inexhaustible resource, solar energy is considered as the most ideal candidate to solve the energy crisis. However, the low energy conversion efficiency is the main drawback of solar cells. Therefore, carbon nitrides, an analog of graphite with special electronic properties, have attracted significant attention as promising photocatalysts [6].

The hardness of β-C_3N_4 is similar to that of a diamond [7–9]. C_3N_4 requires cheap raw materials and has excellent chemical stability [10–13]. According to Liu and Cohen [8], the compressibility of C_3N_4 is similar to that of a diamond. According to Xu and Gao [14], pseudocubic-C_3N_4 is a direct band semiconductor, whereas its other three dense forms (α-, β-, and cubic phases) are indirect bandgap semiconductors. They used an approximation method to determine the band gaps of different C_3N_4 phases. As the band gaps of α-, β-, and cubic phases are too large, they are not suitable for visible light absorption. Multifarious attempts, such as the construction of sundry nano-architectures [15], surface modification [16], heterojunction manufacturing [17], and chemical doping [18,19], have been made to improve the optical properties of C_3N_4.

The optical properties of pure graphitic-C_3N_4 can be improved through the doping of different transition metals (Cu^{2+}, Fe^{3+}, Co^{3+}, and Ni^{2+}) because this phenomenon allows them to be located in the cavities between adjacent tri-s-triazine units on the same π-conjugated planes [20,21]. Wan et al. [22] studied the photocatalytic degradation performance of La-intercalated g-C_3N_4 toward Rhodamine B. However, the structure of La-doped C_3N_4 was not clear, and the photocatalysis mechanism was not properly understood. Methylene blue (MB) is a safe drug and causes no toxicity when its therapeutic dose limit is <2 mg/kg. A female patient with breast cancer experienced sentinel lymph node biopsy localization during MB peritumor injection and, consequently, skin, and fat necroses were developed, followed by dry skin gangrene [23]. MB also causes a hemolytic anemia with severe renal insufficiency and deficiency of glucose-6-phosphate dehydrogenase (G6PD). MB also interferes with the light emission of a pulse oximeter, resulting in a false depression in the oxygen saturation reading [24]. Rare-earth materials are a smart class of dopants because they can easily give trivalent cations, thus altering the structures, and characteristics of nanoparticles and creating multifunctional materials due to their f-electronic configurations. Lanthanum (La) is widely used in aircraft as an activator of the propellant burning rate and also as a laser material in screens, phosphorus, and ceramics intensifying X-ray imaging. Lanthanum orthoferrite ($LaFeO_3$) with a perovskite structure exhibits p-type conductivity at high partial oxygen pressure (PO_2 > 10−4 atm) [25]. $LaFeO_3$ is a charge-transfer-type insulator and displays a bandgap of 2.1–2.0 eV [26,27]. Industrial wastewater pollution has become a considerably complex problem due to the growing diversity of products and precursor chemicals disposed of in water resources [28]. Photocatalytic oxidation can directly use solar energy to efficiently remove organic contaminants [29]. Phenol is one of the most widely used toxic recalcitrant organic compounds in petrochemical, pharmaceutical, and chemical industries [30]. Dyes are highly toxic and extremely poisonous, even at small concentrations [31]. However, pigments and dyes are widely used in manufacturing textiles, paper, plastics, leather, foods, and cosmetic goods, although the release of their wastes into water leads to major dangers to the aquatic environment [32].

In the present study, pure g-C_3N_4, and different concentrations of La-doped C_3N_4 were synthesized by a facile combustion method. The physicochemical characteristics of the as-prepared samples were investigated by X-ray diffraction, scanning electron microscopy (SEM), UV-vis spectrometry. The visible-photocatalytic degradation activities of pure g-C_3N_4 and La-doped g-C_3N_4 toward MB and phenol were analyzed.

2. Experimental and characterization methods

2.1. Reagents

Analytical grade melamine, lanthanum nitrate ($La(NO_3)_3 \cdot 6H_2O$), and other chemicals were purchased from Sigma-Aldrich, (Hamburg, Germany) and were used without further purification. In order to avoid contamination, deionized water was used for the preparation and washing of materials at a resistivity of ~18 MΩ cm.

2.2. Preparation of pure porous graphitic-C_3N_4 and La-doped C_3N_4

Pure graphitic-C_3N_4 was prepared through the air atmospheric pyrolysis of melamine. Urea (8 g) was ground in a crucible, heated to 550°C at a rate of 5°C/min, finally, tempered in the flowing air at 550°C for 2 h. The sample was then allowed to cool down to room temperature. The resulting powder was then ground with a mortar pestle. Residues absorbed on the porous g-C_3N_4 surface were removed by deionized water. In order to synthesize the doped sample, $La(NO_3)_3 \cdot 6H_2O$ was added to melamine in the first stage, and the other procedures for pure C_3N_4 were then repeated.

2.3. Characterizations

The structural analysis of pure C_3N_4 and La-doped C_3N_4 was performed by XRD. The XRD analysis was carried out by an X-ray diffractometer (Shimadzu LabXRD-6000, Tokyo, Japan) under Cu-K_α radiation (λ = 1.5406 Å) at 30 kV and 30 mA.

The morphologies of the samples were observed by SEM (Model: JSM-6360) at an operating voltage of 20 kV.

The optical diffused reflectance spectra of the samples were detected by a UV-vis-NIR spectrophotometer (JASCO UV-vis-NIR-V-57, Easton, USA) in the wavelength range of 200−800 nm.

The samples were irradiated under visible light to observe their photocatalytic degradation activities toward phenol and MB aqueous solutions in a handmade photo-reactor. This photo-reactor was composed of two parts: the outer part was a wooden box of 100 cm height and 65 cm width, whereas the inner part contained eight visible lamps, each one of 18 W, 60 cm length, emitting light at

425–600 nm. The samples were put in a beaker with 50 mL of MB (20 mg/L) and were exposed to darkness to study the chemisorption for 30 min. Phenol (100 mL, 300 ppm) was exposed to light in the presence of the samples. The samples were then irradiated under visible light, and their activities were noted for every 15 min. The samples were finally analyzed by a 160 A UV-vis-spectrophotometer.

The removal rate [Rev (%)] of photodegrading MB in the aqueous solution was calculated by the following formula:

$$\text{Rev}(\%) = \left(1 - \frac{C}{C_0}\right) \times 100\% \quad (1)$$

where C_0 and C (mg/L) are the initial and final concentrations of photodegrading MB. The obtained photodegradation data from different catalysts obeyed the first-order kinetics, $\ln(C/C_0) = kt$, where k is the first-order rate constant.

3. Results and discussion

3.1. XRD analysis of pure g-C_3N_4 and La-doped g-C_3N_4

The XRD spectra of the pure and doped samples with different La^{3+} concentrations (0.001, 0.01, 0.1, 0.5, and 1.0 g) are displayed in Fig. 1. For the pure g-C_3N_4 sample, both the (100) peak at 2θ = 13.10°and the (002) peak at 2θ = 27.50° were less intense [33,34], and it can be attributed to the interlayer stacking reflection of the conjugated aromatic system and the interplanar structural packing. The (002) peak indicates the denser packing of C_3N_4 molecules. The diffraction peak at 2θ = 13.1° disappeared with the increasing doping content of La ions, and the main peak of g-C_3N_4 at 2θ = 27.845° overlapped with the (012) plane at 2θ = 27.58°. Moreover, a new peak at 2θ = 47.15° appeared from the plane (111) when the La doping content was 1.0 g, and this result confirms that La^{3+} ions were successfully incorporated on the surface of g-C_3N_4. The (100) peak gradually disappeared with the increase of the doping concentration. It indicates that La was homogeneously doped into the g-C_3N_4 lattice although most of La was confined on the surface of C_3N_4.

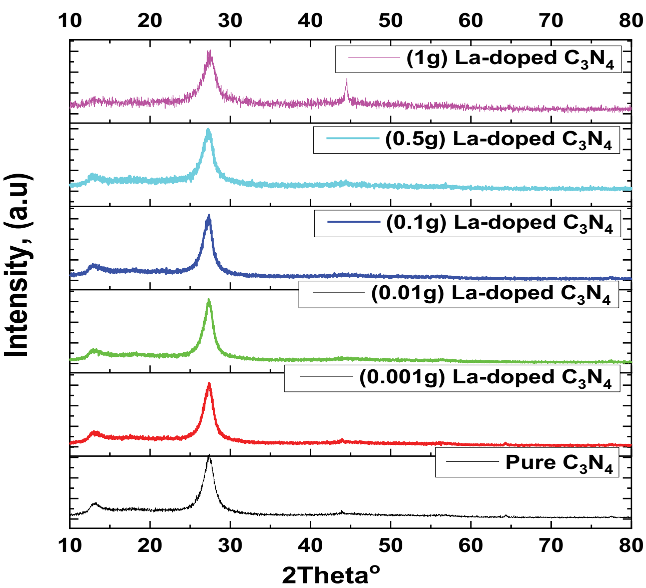

Fig. 1. XRD distributions of pure g-C_3N_4 and La nitrate ions doped g-C_3N_4 samples with various amounts of La (0.001, 0.01, 0.1, 0.5, and 1.0 g La).

3.2. SEM analysis of pure C_3N_4 and La-doped C_3N_4

The surface morphologies of pure g-C_3N_4 and La-doped g-C_3N_4 are exhibited in Fig. 2. The pure g-C_3N_4 sample possessed some granular aggregates. The surface of pure g-C_3N_4 appeared to be very rough, and no ordered structure was observed in it (Fig. 2a). Fig. 2b displays single crystals with a distinct hexagonal morphology. It is noticeable from Fig. 2f that the 1.0 g La-doped g-C_3N_4 sample had disordered sheets. The diameter of La-doped g-C_3N_4 ranged between 6.11 and 16.08 μm. With the increasing La^{3+} doping concentration, the well-defined particle shape became ambiguous, and the particle size gradually decreased.

3.3. UV-vis diffused reflectance measurements of pure C_3N_4 and La-doped C_3N_4

The bandgaps of the pure and doped samples were determined by UV-vis diffused reflectance spectroscopy, and their reflection spectra ($R(\lambda)$) were detected. The intensities of optical reflection spectra increased with the increasing wavelength and decreased with the increasing La concentration. The absorption edge of La-doped g-C_3N_4 had a slight redshift in comparison to pure g-C_3N_4 (Fig. 3). Fig. 4 presents the energy bandgaps of the as-prepared materials estimated from the plot of $(\alpha h\upsilon)^{1/2}$ vs. the incident photon energy (hυ) based on Tauc's formula [35]. The Kubelka–Munk function and its related absorption coefficient (α) were used to determine the bandgap [36,37].

$$(\alpha h\upsilon) = \frac{(F(R)h\upsilon)}{d} = A\left(h\upsilon - E_g\right)^n \quad (2)$$

where A is a pre-factor, E_g is the energy bandgap, and n provides information about the type of transition (n = 2 for the indirect bandgap and n = 1/2 for the direct bandgap). The plots of $(\alpha h\upsilon)^2$ vs. hυ for the pure and La-doped g-C_3N_4 samples are displayed in Fig. 5. The linear portions of the plots were extrapolated to measure the bandgap. The estimated band gaps of the pure and La-doped g-C_3N_4 samples are summarized in Table 1. The direct bandgap decreased from 2.714 for pure g-C_3N_4 to 2.638 for 1.0 g La-doped g-C_3N_4; however, the indirect bandgap decreased from 2.891 to 2.872 with the same ratio of La. The photocatalytic activity of La-doped g-C_3N_4 was enhanced because La nitrate ions contributed to the narrowing of the bandgap energy.

3.4. Photocatalytic activity analysis

Some contradictory opinions have been proposed concerning the photocatalytic degradation of dyes and azo-dyes [38,39]. According to Wang et al. [40], some dyes can absorb visible light during photodegradation.

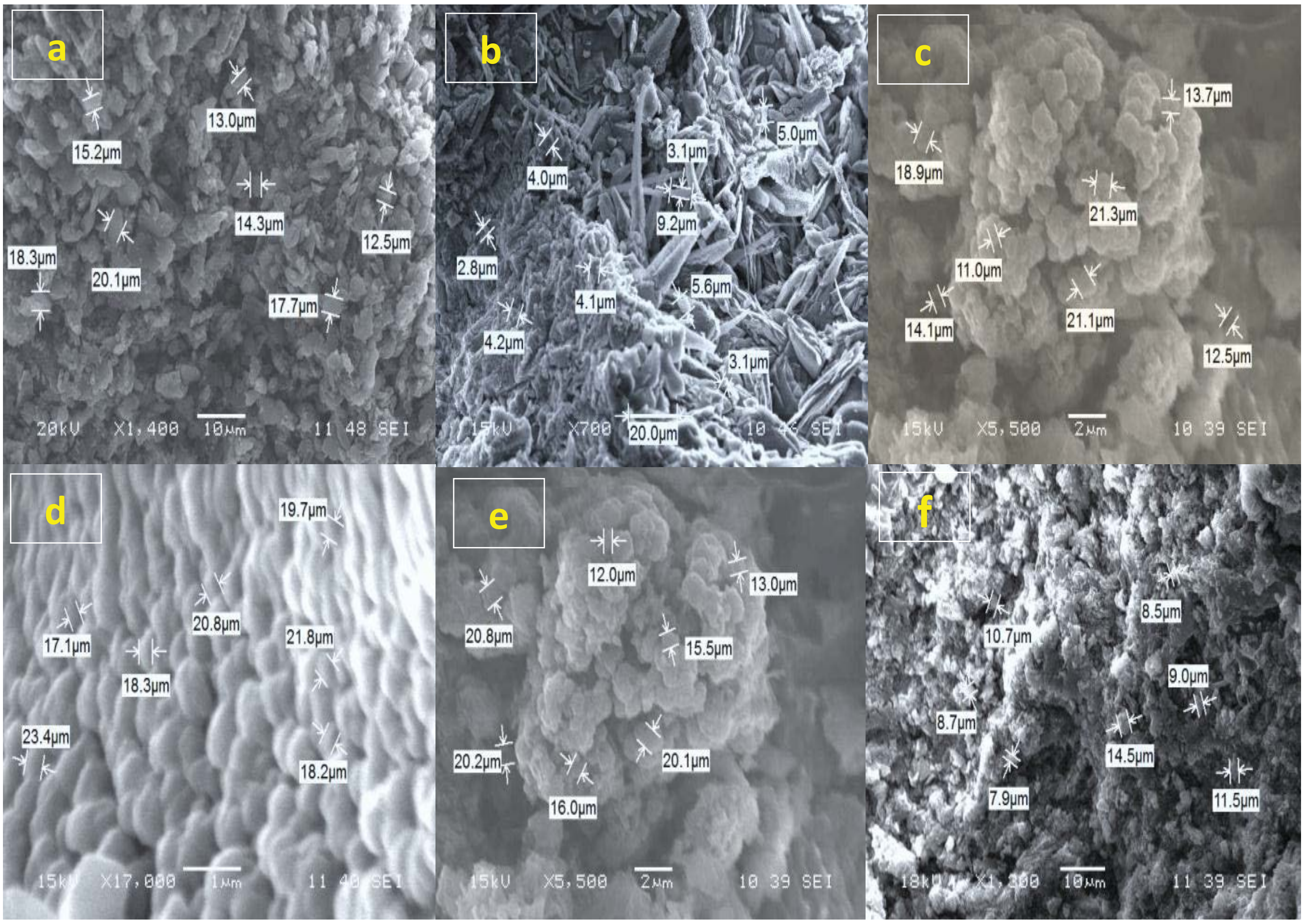

Fig. 2. SEM micrographes of (a) pure g-C_3N_4, (b) 0.001 La-C_3N_4, (c) 0.01 La-C_3N_4, (d) 0.1 La-C_3N_4, (e) 0.5 La-C_3N_4, and (f) 1 La-C_3N_4.

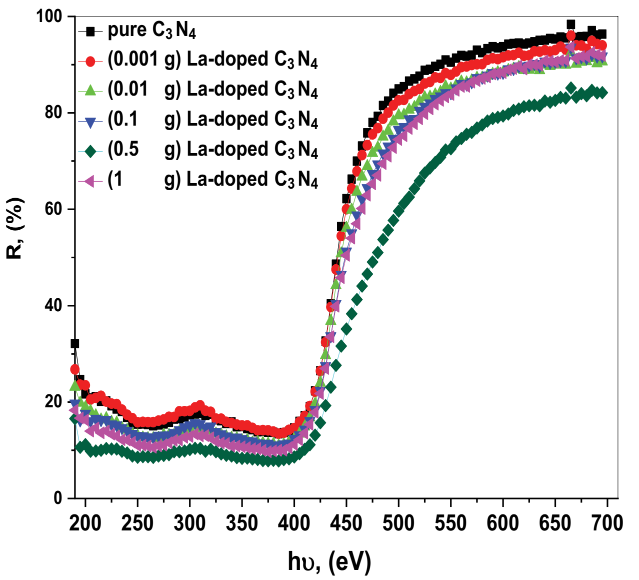

Fig. 3. UV-vis diffused reflectance of pure g-C_3N_4 and La doped g-C_3N_4 samples with various La ion concentrations.

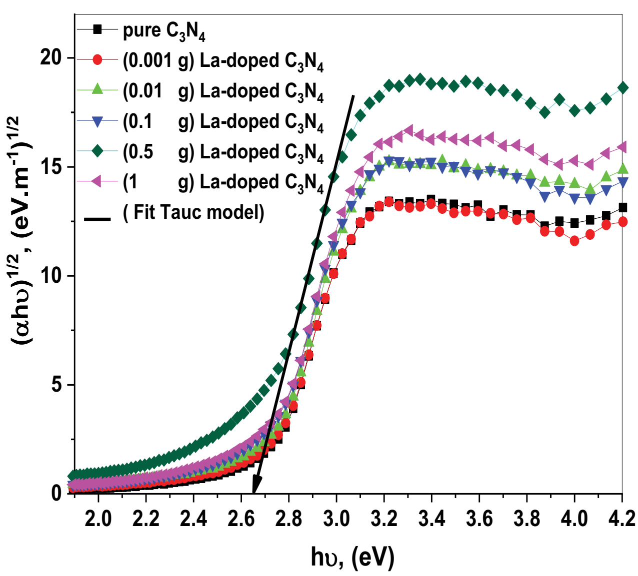

Fig. 4. Plots of $(\alpha h\upsilon)^{1/2}$ vs. the incident photon energy hυ for the investigated samples.

The initial levels of MB and phenol concentrations remained almost the same in the dark for all samples, suggesting that photocatalytic charge segregation played a major role in improving the photocatalytic effectiveness [41]. Under the same experimental conditions, the effectiveness of photolysis without a photocatalyst was negligible and phenol and MB were stable under visible light irradiation. The photocatalytic performances of the pure and La-doped g-C_3N_4 samples are presented in Fig. 6. It is discernible that the doped samples exhibited better photodegradation efficiency for both MB and phenol. The obtained rate constant values are presented in Table 2 and Fig. 7. The rate constant for La-doped g-C_3N_4 was greater than that of pure g-C_3N_4, indicating that the g-C_3N_4 catalyst maintained good catalytic stability in the photocatalytic reaction. It indicates that the photodegradation of MB and phenol decreased by the photocatalytic reaction. The obtained photodegradation data for different catalysts obeyed the first-order kinetics, $\ln(C/C_0) = kt$, where k is the first-order rate constant. It was observed that at $t = 0$, the dye concentration was constant, indicating the absence of chemisorption. The rate constant increased from 0.00272 for pure g-C_3N_4 to 0.00763 for La-doped g-C_3N_4. Moreover, the photodegradation rate of phenol was higher than that of MB for both samples. The rate constant increased from 0.01406 for pure g-C_3N_4 to 0.1025 for La-doped g-C_3N_4 [42]. In comparison to other photocatalysts [39,43,44], La-doped g-C_3N_4 manifested an improved visible-light photocatalytic activity toward MB and phenol. In comparison to g-C_3N_4, La/g-C_3N_4 had better visible-light absorption, absorptivity, and photocurrent response.

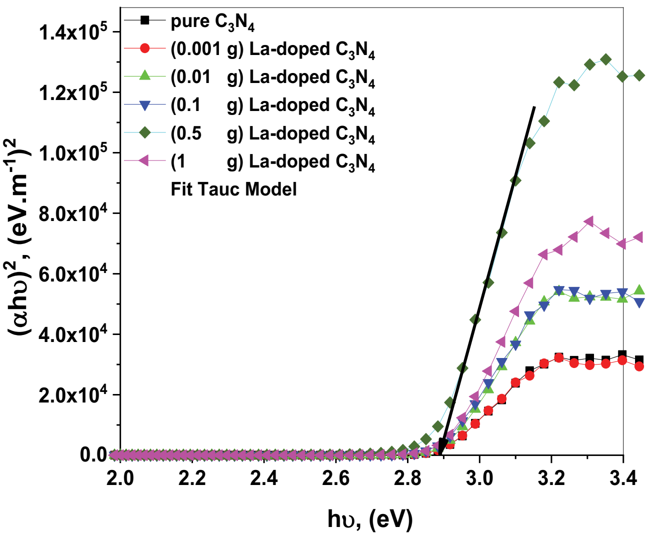

Fig. 5. Plots of $(\alpha h\upsilon)^{1/2}$ vs. the incident photon energy $h\upsilon$ for the as-prepared samples.

3.5. Photocatalytic mechanism

The photocatalytic mechanism depends on the wavelength of the illuminated light, pollutant, and the photocatalyst. When the semiconductor absorbs the energy of light that was higher than the energy gap, the electron is pumped from the conduction band to the energy of the outer valence band, creating a hole. Electrons in the conduction band could reduce the dye or react with dissolved oxygen species to form superoxide ions (O_2^-) or react with electron acceptors (O_2) absorbed on the catalyst surface. Holes can oxidize water molecules into OH^- radicals or react with OH^-. Together with other high oxidant species (peroxide radicals), holes are responsible for the heterogeneous catalytic photodecomposition of organic substrates (dyes). The generation of OH. radicals were strongly affected by edge position of the valence band semiconductor that lead to oxidize Methylene Blue dye into mineral products [45]. Yang et al. [46] proposed a possible photocatalytic mechanism over the Ti_3C_2/porous g-C_3N_4 Schottky junction and determined the work functions of Ti_3C_2 and porous g-C_3N_4 as 3.31 and 2.53 eV, respectively. When Ti_3C_2 and porous g-C_3N_4 were in contact, visible-light-induced electrons on porous g-C_3N_4 flowed to Ti_3C_2 at the lower energy level to achieve an equilibrium state between the Fermi levels of Ti_3C_2 and porous g-C_3N_4. A space charge layer was generated on the side of porous g-C_3N_4, causing the upward bending of the energy band and the formation of a Schottky barrier. Electrons trapped by Ti_3C_2 could not flow back to the conduction band (CB) of porous g-C_3N_4, thus efficiently boosting the spatial charge separation. Therefore, Ti_3C_2 nanosheets created a Schottky junction with the host porous g-C_3N_4 nanosheets to improve the photocatalytic activity.

Table 2
Rate constant values for the pure g-C_3N_4 and La-doped g-C_3N_4 with various mass of La-ions

Samples	MB	Phenol
Pure CN	0.00272	0.01406
0.001 % La-doped CN	0.00296	0.01868
0.01 % La-doped CN	0.00324	0.03222
0.1 % La-doped CN	0.00547	0.05103
0.5 % La-doped CN	0.00852	0.09557
1 % La-doped CN	0.00763	0.10258

Table 1
Direct and indirect band gap energy of the investigated samples

Samples	Pure C_3N_4	0.001 g La-doped C_3N_4	0.01 g La-doped C_3N_4	0.1 g La-doped C_3N_4	0.5 g La-doped C_3N_4	1 g La-doped C_3N_4
Direct bandgap	2.714	2.709	2.707	2.686	2.683	2.638
Indirect bandgap	2.891	2.887	2.883	2.880	2.876	2.872

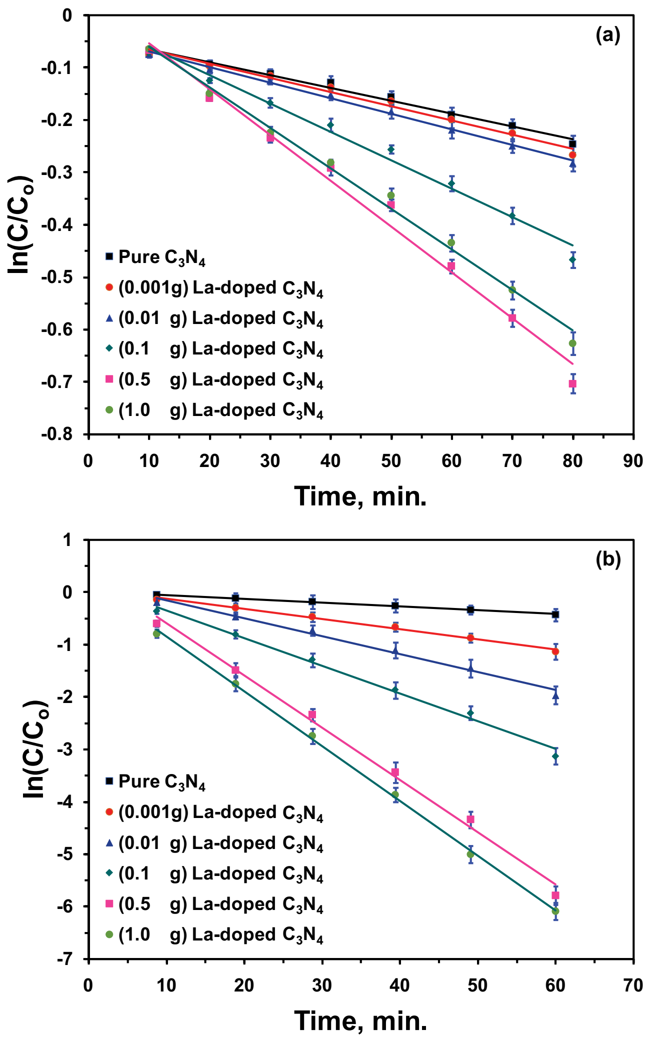

Fig. 6. (a and b) Effect of photodegrading MB dye on the first order kinetic adjustment curves of the photocatalytic samples.

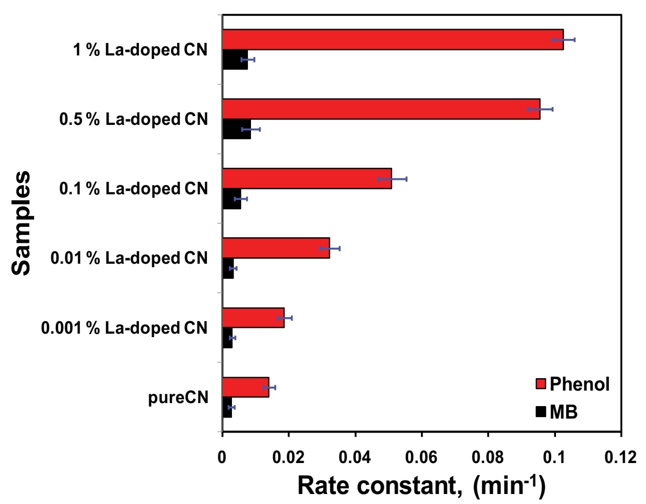

Fig. 7. MB evolution rate constants during photocatalytic degradation for the samples under visible light irradiation.

The photodegradation of phenol occurs in two primary phases [47]. In the first stage, phenol is degraded to complicated hydroxylates (benzoquinone, catechol, and biphenyl-4-ol) and short-chain compounds. These compounds become mineralized to CO_2 and H_2O during the mineralization period [48]. This phase has a significant impact on the breakdown of easy hydrocarbons, such as glycerol, formic acid, oxalic acid, butanol, ethylene, and acetyl acid [49]. Huan Yia et al. [50] synthesized biomimetic hemin bismuth tungstate (HBWO) [2D] and found that the introduction of hemin promoted the photocatalytic activity of 2D BWO. HBWO became immobilized in monomer hemin on the surface of 2D BWO through a simple hydrothermal process. Tetracycline (TC) photodegradation has also been studied using HBWO composites. 2D nano-structured HBWO composites are considered as a promising photocatalytic substrate for environment-friendly photodegradation. Ali et al. [51] applied TiO_2 nanotubes doped by bismuth in 50 mg L^{-1} phenol visible-degradation to reach 17.5% phenol degradation.

4. Conclusion

Pure and La nitrate ions-doped g-C_3N_4 were synthesized through the air atmospheric pyrolysis of melamine. The XRD analysis confirmed that loaded La nitrate ions were homogeneously incorporated and confined on the surface of g-C_3N_4. SEM images revealed that the well-defined particle shape became ambiguous and the particle size gradually decreased with the increasing doping amount of La nitrate ions. All UV-vis reflectance spectra decreased with the increasing doping amount of La nitrate ions on g-C_3N_4. Under visible light irradiation, La-doped g-C_3N_4 exhibited higher photodegradation efficiency toward MB in comparison to pure g-C_3N_4.

Acknowledgments

The authors express their appreciation to the Deanship of Scientific Research at King Khalid University for funding this work through the Project for Group Research under grant number (R.G.P. 337/40).

References

[1] H. Montigaud, B. Tanguy, G. Demazeau, I. Alves, S. Courjault, C_3N_4: dream or reality? Solvothermal synthesis as macroscopic samples of the C_3N_4 graphitic form, J. Mater. Sci., 35 (2000) 2547–2552.
[2] D.R. Miller, J. Wang, E.G. Gillan, Rapid facile synthesis of nitrogen-rich carbon nitride powders, J. Mater. Chem., 12 (2002) 2463–2469.
[3] D.M. Teter, R.J. Hemley, Low-compressibility carbon nitrides, Science, 271 (1996) 53–55.
[4] X.A. Zhao, C.W. Ong, Y.C. Tsang, Y.W. Wong, P.W. Chan, C.L. Choy, Reactive pulsed laser deposition of CN_x films, Appl. Phys. Lett., 66 (1995) 2652–2654.
[5] Y. Zhang, H. Gao, Y. Gu, Structure studies of C_3N_4 thin films prepared by microwave plasma chemical vapour deposition, J. Phys. D: Appl. Phys., 34 (2001) 299–302.
[6] G. Dong, Y. Zhang, Q. Pan, J. Qiu, A fantastic graphitic carbon nitride (g-C_3N_4) material: electronic structure, photocatalytic and photoelectronic properties, J. Photochem. Photobiol., C, 20 (2014) 33–50.

[7] M.L. Cohen, Calculation of bulk moduli of diamond and zinc-blende solids, Phys. Rev. B, 32 (1985) 7988–7991.
[8] A.Y. Liu, M.L. Cohen, Prediction of new low compressibility solids, Science, 245 (1989) 841–842.
[9] A.Y. Liu, M.L. Cohen, Structural properties and electronic structure of low-compressibility materials: beta-Si_3N_4 and hypothetical beta-C_3N_4, Phys. Rev. B, 41 (1990) 10727–10734.
[10] D.L. Jiang, L.L. Chen, J.J. Zhu, M. Chen, W.D. Shi, J.M. Xie, Novel p-n heterojunction photocatalyst constructed by porous graphite-like C_3N_4 and nanostructured BiO: facile synthesis and enhanced photocatalytic activity, Dalton Trans., 42 (2013) 15726–15734.
[11] X.C. Wang, K. Maeda, A. Thomas, K. Takanabe, G. Xin, J.M. Carlsson, A metal-free polymeric photocatalyst for hydrogen production from water under visible light, Nat. Mater., 8 (2009) 76–79.
[12] S.C. Yan, Z.S. Li, Z.G. Zou, Photodegradation performance of g-C_3N_4 fabricated by directly heating melamine, Langmuir, 25 (2009) 10397–10401.
[13] X. Dong, F. Cheng, Recent development in exfoliated two-dimensional g-C_3N_4 nanosheets for photocatalytic applications, J. Mater. Chem. A, 3 (2015) 23642–23652.
[14] Y. Xu, S.-P. Gao, Bandgap of C_3N_4 in the GW approximation, Int. J. Hydrogen Energy, 37 (2012) 11072–11080.
[15] Y. Zheng, L.H. Lin, X.J. Ye, F.S. Guo, X.C. Wang, Helical graphitic carbon nitrides with photocatalytic and optical activities, Angew. Chem. Int. Ed., 53 (2014) 11926–11930.
[16] M. Groenewolt, M. Antonietti, Synthesis of g-C_3N_4 nanoparticles in mesoporous silica host matrices, Adv. Mater., 17 (2005) 1789–1792.
[17] C.S. Pan, J. Xu, Y.J. Wang, D. Li, Y.F. Zhu, Dramatic activity of C_3N_4/$BiPO_4$ photocatalyst with core/shell structure formed by self-assembly, Adv. Funct. Mater., 22 (2012) 1518–1524.
[18] S.C. Yan, Z.S. Li, Z.G. Zou, Photodegradation of rhodamine B and methyl orange over boron-doped g-C_3N_4 under visible light irradiation, Langmuir, 26 (2010) 3894–3901.
[19] Y.J. Zhang, T. Mori, J.H. Ye, M. Antonietti, Phosphorus-doped carbon nitride solid: enhanced electrical conductivity and photocurrent generation, J. Am. Chem. Soc., 132 (2010) 6294–6295.
[20] L. Xu, J.X. Xia, H. Xu, J. Qian, J. Yan, L.G. Wang, K. Wang, H.M. Li, AgX/graphite-like C_3N_4 (X = Br, I) hybrid materials for photoelectrochemical determination of copper(II) ion, Analyst, 138 (2013) 6721–6726.
[21] Q. Liu, J.Y. Zhang, Graphene supported Co-g-C_3N_4 as a novel metal macrocyclic electrocatalyst for the oxygen reduction reaction in fuel cells, Langmuir, 29 (2013) 3821–3828.
[22] J. Wan, S.Z. Hu, F.Y. Li, Z.P. Fan, F. Wang, J. Zhang. Synthesis of CL doped g-C_3N_4 with enhanced photocatalytic activity under visible light, Asian J. Chem., 26 (2014) 8543–8546.
[23] C. Jack II, L. Jerrold B, Methylene blue, Am. J. Ther., 10 (2003) 289–91.
[24] M. Salhab, W. Al Sarakbi, K. Mokbel, Skin and fat necrosis of the breast following methylene blue dye injection for sentinel node biopsy in a patient with breast cancer, Int. Semin. Surg. Oncol., 2 (2005) 26–29.
[25] I. Wærnhus, P.E. Vullum, R. Holmestad, T. Grande, K. Wiik, Electronic properties of polycrystalline $LaFeO_3$. Part I: experimental results and the qualitative role of Schottky defects, Solid State Ionics, 176 (2005) 2783–2790.
[26] T. Arima, Y. Tokura, J.B. Torrence, Variation of optical gaps in perovskite-type 3d transition-metal oxides, Phys. Rev. B, 48 (1993) 17006–17009.
[27] A. Chainani, M. Mathew, D.D. Sarma, Electronic structure of $La_{1-x}SrxFeO_3$, Phys. Rev. B, 48 (1993) 14818–14825.
[28] Y. Li, K. Lv, W. Ho, Z. Zhao, Y. Huang, Enhanced visible-light photo-oxidation of nitric oxide using bismuth-coupled graphitic carbon nitride composite heterostructures, Chin. J. Catal., 38 (2017) 321–329.
[29] J. Wen, J. Xie, Z. Yang, R. Shen, H. Li, X. Luo, X. Chen, X. Li, Fabricating the robust g-C_3N_4 nanosheets/carbons/NiS multiple heterojunctions for enhanced photocatalytic H_2 generation: an insight into the trifunctional roles of nano carbons, ACS Sustainable Chem. Eng., 5 (2017) 2224–2236.
[30] J. Tauc, R. Grigorovici, A. Vaucu, Optical properties and electronic structure of amorphous germanium, Phys. Status Solidi B, 15 (1966) 627–637.
[31] I.S. Yahia, H.Y. Zahran, F.H. Alamri, Pyronin Y as new organic semiconductors: structure, optical spectroscopy and electrical/dielectric properties, Synth. Met., 218 (2016) 19–26.
[32] H. Eskandarloo, A. Badiei, C. Haug, Enhanced photocatalytic degradation of an azo textile dye by using TiO_2/NiO coupled nanoparticles: optimization of synthesis and operational key factors, Mater. Sci. Semicond. Process., 27 (2014) 240–253.
[33] Y.P. Bhoi, B.G. Mishra, Photocatalytic degradation of alachlor using type-II CuS/ $BiFeO_3$ heterojunctions as novel photocatalyst under visible light irradiation, Chem. Eng. J., 344 (2018) 391–401.
[34] I. Prabha, S. Lathasree, Photodegradation of phenol by zinc oxide, titania and zinc oxide–titania composites: nanoparticle synthesis, characterization and comparative photocatalytic efficiencies, Mater. Sci. Semicond. Process., 26 (2014) 603–613.
[35] S. Waclawek, H.V. Lutze, K. Grubel, V.V.T. Padil, M. Cernik, D.D. Dionysiou, Chemistry of persulfates in water and wastewater treatment: a review, Chem. Eng. J., 330 (2017) 44–62.
[36] D.R. Shinde, P.S. Tambade, M.G. Chaskar, K.M. Gadave, Photocatalytic degradation of dyes in water by analytical reagent grades ZnO, TiO_2 and SnO_2: a comparative study, Drinking Water Eng. Sci., 10 (2017) 109–117.
[37] Z. Jin, R. Hu, H. Wang, J. Hu, T. Ren, One-step impregnation method to prepare direct Z-scheme $LaCoO_3$/g-C_3N_4 heterojunction photocatalysts for phenol degradation under visible light, Appl. Surf. Sci., 491 (2019) 432–442.
[38] B. Zhao, S. Ge, D. Pan, Q. Shao, J. Lin, Z. Wang, Z. Hu, T. Wu, Z. Guo, Solvothermal synthesis, characterization and photocatalytic property of zirconium dioxide doped titanium dioxide spinous hollow microspheres with sunflower pollen as bio-templates, J. Colloid Interface Sci., 529 (2018) 111–121.
[39] J. Yu, G. Dai, Q. Xiang, M. Jaroniec, Fabrication and enhanced visible-light photocatalytic activity of carbon self-doped TiO_2 sheets with exposed 001 facets, J. Mater. Chem., 21 (2011) 1049–1057.
[40] Q. Wang, H. Jiang, S. Zang, J. Li, Q. Wang, Gd, C, N and P quaternary doped anatase-TiO_2 nano-photocatalyst for enhanced photocatalytic degradation of 4-chlorophenol under simulated sunlight irradiation, J. Alloys Compd., 586 (2014) 411–419.
[41] T.K. Mandal, S.P.K. Malhotra, R.K. Singha, Photocatalytic degradation of methylene blue in presence of ZnO nanopowders synthesized through a green synthesized method, Rom. J. Mater., 48 (2018) 32–38.
[42] M. Asadollahi-Baboli, Exploring QSTR analysis of the toxicity of phenols and thiophenols using machine learning methods, Environ. Toxicol. Pharmacol., 34 (2012) 826–831.
[43] D.P. Zagklis, A.I. Vavouraki, M.E. Kornaros, C.A. Paraskeva, Purification of olive mill wastewater phenols through membrane filtration and resin adsorption/desorption, J. Hazard. Mater., 285 (2015) 69–76.
[44] Y. Huan, J. Min, H. Danlian, Z. Guangming, L. Cui, Q. Lei, Z. Chengyun, L. Bisheng, L. Xigui, C. Min, X. Wenjing, X.Z. Chen, Advanced photocatalytic Fenton-like process over biomimetic hemin-Bi_2WO_6 with enhanced pH, J. Taiwan Inst. Chem. Eng., 93 (2018)184–192.
[45] K. Li, Y. Liang, J. Yang, Q. Gao, Y. Zhu, S. Liu, R. Xu, X. Wu, Controllable synthesis of {001} facet dependent foursquare BiOCl nanosheets: a high efficiency photocatalyst for degradation of methyl orange, J. Alloys Compd., 695 (2017) 238–249.
[46] Y. Yang, Z. Zeng, G. Zeng, D. Huang, R. Xiao, C. Zhang, C. Zhou, W. Xiong, W. Wang, M. Cheng, W. Xue, H. Guo, X. Tang, D. He, Ti_3C_2 Mxene/porous g-C_3N_4 interfacial Schottky junction for boosting spatial charge separation in photocatalytic H_2O_2 production, Appl. Catal., B, 258 (2019) 117956–117968.

[47] T.T.T. Dang, S.T.T. Le, D. Channe, W. Khanitchaidecha, A. Nakaruk, Photodegradation mechanisms of phenol in the photocatalytic process, Res. Chem. Intermed., 42 (2016) 5961–5974.
[48] Y. Ao, J. Bao, P. Wang, C. Wang, J. Hou, Bismuth oxychloride modified titanium phosphate nanoplates: a new *p-n* type heterostructured photocatalyst with high activity for the degradation of different kinds of organic pollutants, J. Colloid Interface Sci., 476 (2016) 71–78.
[49] N.K. Vel Leitner, M. Dore, Hydroxyl radical induced decomposition of aliphatic acids in oxygenated and deoxygenated aqueous solutions, J. Photochem. Photobiol., A, 99 (1996) 137–143.
[50] H. Yia, M. Yana, D. Huang, G. Zeng, C. Lai, M. Li, X. Huo, L. Qin, S. Liu, X. Liu, B. Li, H. Wang, M. Shen, Y. Fu, X. Guo, Synergistic effect of artificial enzyme and 2D nano-structured Bi_2WO_6 for eco-friendly and effcient biomimetic photocatalysis, Appl. Catal., B, 250 (2019) 52–62.
[51] I. Ali, S.-R. Kim, S.-P. Kim, J.-O. Kim, Anodization of bismuth doped TiO_2 nanotubes composite for photocatalytic degradation of phenol in visible light, Catal. Today, 282 (2017) 31–37.